

A Second Intense Burst with Photospheric Radius Expansion from X2127+119 in M15

Alan P. Smale¹

Laboratory for High Energy Astrophysics, Code 662, NASA/Goddard Space Flight Center, Greenbelt, MD 20771

ABSTRACT

In 2000 September we observed a bright X-ray burst from X2127+119 with the *Rossi X-ray Timing Explorer*. This burst has a multi-peaked profile, a peak luminosity of $\sim 6.5 \times 10^{38}$ erg s $^{-1}$, a total integrated energy of $\sim 2 \times 10^{40}$ ergs, and significant photospheric radius expansion to a maximum extent of $R=118 \pm 5$ km. From the luminosity-temperature relation during the expansion phase we derive estimates for the gravitational redshift at the neutron star surface, the corrected Eddington luminosity, and the neutron star mass. We detect no slow (~ 30 s) radial oscillations or fast (100–1200 Hz) coherent oscillations or QPO during the burst.

The 2000 September event is only the second burst ever observed from this globular cluster binary (in M15 = NGC 7078), and it shares many characteristics with the event detected by Ginga in 1988 October (Dotani et al. 1990; van Paradijs et al. 1990), the key difference probably being the total amount of material consumed in the thermonuclear flash.

Subject headings: accretion, accretion disks — binaries: close — stars: individual (X2127+119) — stars: neutron — X-rays: bursts — X-rays: stars

¹Also Universities Space Research Association.

1. Introduction

The X-ray source X2127+119 is a bright low-mass binary located within 2" of the core of the globular cluster M15 (=NGC 7078). It is identified with the V~15 optical star AC211 (Aurière et al. 1984), which is far and away the brightest counterpart of any globular cluster X-ray source. When folded on the 17.11-hr optical period (Ilovaisky et al. 1993; Homer & Charles 1998), the light curve of X2127+119 shows a broad symmetrical \sim 5-hr eclipse at phase $\phi=0$, and the largest orbital modulation seen from any X-ray binary (1.8 mag in U), but with extremely erratic and complex X-ray and optical behavior between phases $\phi=0.2$ –0.7. Combining this variability with its low L_x/L_{opt} ratio of \sim 20, the natural conclusion is that X2127+119 is an accretion disk corona (ADC) source observed at a sufficiently high inclination that the bulk of the direct X-ray emission is obscured by azimuthal disk structure. However, the detection of a very luminous X-ray burst from the source with the Ginga satellite (Dotani et al. 1990; van Paradijs et al. 1990; hereafter “the 1988 burst”) not only revealed that the compact object must be a neutron star, but also that it must be viewed directly with no intervening obscuration.

The 1988 burst from X2127+119 had a long duration (in excess of 150s), a peak luminosity of 5.1×10^{38} erg s $^{-1}$, and a total energy release of 6.3×10^{40} ergs (correcting the distance to 10.4 kpc; see below), placing it amongst the brightest of the observed Type I X-ray bursts. A bright precursor was seen 6 seconds prior to the main event, and spectral fitting revealed strong photospheric radius expansion during the burst, followed by contraction and a cooling phase. In the first 30s of this contraction, slow radius oscillations occurred (Dotani et al. 1990; van Paradijs et al. 1990).

Per unit mass, low mass X-ray binaries (LMXBs) are \sim 100 times more likely to be found in globular clusters than in the Galaxy as a whole, and they are almost certainly formed by the tidal capture of compact objects, an efficient process within globular clusters because of the high local number density of stars (Fabian, Pringle, & Rees 1975; Hut et al. 1992). The bursts observed from the 12 known globular cluster LMXBs $> 10^{36}$ erg s $^{-1}$ have a special significance because we have relatively accurate information about (a) their distance, and (b) the elemental abundances of the regions in which they were formed. The M15

cluster has a low mean metallicity of \sim 0.01 Solar (Sneden et al. 1991; Geisler et al. 1992; Harris 1996), although the local metallicity of the accreted material in the X2127+119 system may, of course, have been altered from this by evolutionary effects.

In this Paper, we report the observation and analysis of a second burst from X2127+119, 12 years after the first. The burst reported here shares many of the characteristics of the earlier event, being highly energetic with radius expansion, a high peak luminosity, and a multi-peaked profile; however, its main energy release is of shorter duration, leading to a lower total energy, and no precursor is observed.

2. Observations and Results

We observed X2127+119 with *RXTE* (Bradt, Rothschild, & Swank, 1993) on 2000 August 24 04:36–10:31 UT, and then for a series of pointings spanning 2000 September 17 12:02 UT – September 23 02:36 UT, for an on-source total good time of 150 ksec. The data presented here were obtained using the “Standard 2” mode with 16s time resolution, and an event mode with 16 μ sec time resolution and 64 channels covering the full energy range of the PCA. The PCA consists of five Xe Proportional Counter Units (PCUs) numbered PCUs 0 through 4, with a combined total effective area of about 6500 cm 2 (Jahoda et al. 1996). PCUs 0, 2, and 3 were reliably on throughout the observation, and the data shown here are from these detectors. Data were reduced using the *RXTE* standard analysis software included in FTOOLS 5.0.1, and we used XSPEC 11.0 for our spectral analysis. Where necessary a small instrument-related deadtime correction (6%) has been applied to the derived PCA fluxes. Errors on spectral fit parameters are quoted to 90% confidence.

The burst was observed during the September sequence, at 2000 September 22 13:47:41 UT, a time corresponding to phase $\phi=0.79 \pm 0.03$ in the binary cycle of X2127+119, well away from the partial eclipse. In Figure 1 we show the intensity profile of the burst in the 2–25 keV range. The profile has a complex structure, with an initial fast rise to a first emission peak in <0.5 s, followed by three further peaks in the overall counting rate separated from the first by 3.75s, 11.0s, and 21.5s (all such times in this paper are quoted to ± 0.25 s accuracy unless otherwise stated). The burst took the source from its persistent emission rate of 90 c/s to a maximum of 11,000 c/s,

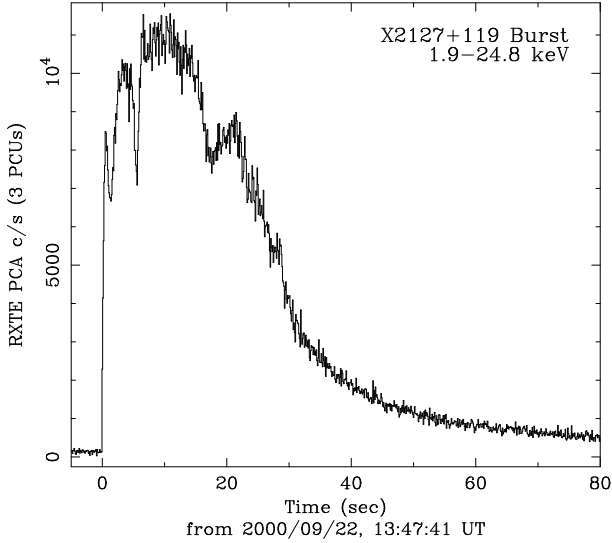


Fig. 1.— The intensity profile of the bright Type I burst observed from X2127+119 in 2000 September, plotted with a time resolution of 0.1s.

after which it decayed with a 1/e-folding time of 30s. The effects of the burst are still visible in the X-ray spectra 300s after its initial rise. A full timing analysis was performed on the burst data: no slow (~ 30 s) radius oscillations or fast (100 Hz–1200 Hz) coherent oscillations or QPO were detected.

The energy dependence of the burst profile is illustrated in Figure 2. In the 1.9–3.5 keV band the initial energy release appears gradual, extending over 6s. At the highest energies the burst appears as a bright 1s pulse, followed by a more gradual 20s rise and an almost-symmetrical decay. Such energy-dependent double peaking in Type I bursts has long been recognized as the signature of photospheric radius expansion in bursts reaching the Eddington luminosity (Hoffman, Cominsky, & Lewin 1980; Lewin, van Paradijs, & Taam 1993).

To study the physical morphology of the burst in more detail, we extracted a series of spectral slices through the event with a time resolution of 0.25s, and performed spectral fits to them over the 2.5–15 keV energy range. Our first pass ultimately proved to be the most satisfactory: we fit a simple blackbody function to the burst spectra, using as background a 300s section of persistent-emission data from immediately prior to the burst. Experimentation showed that the

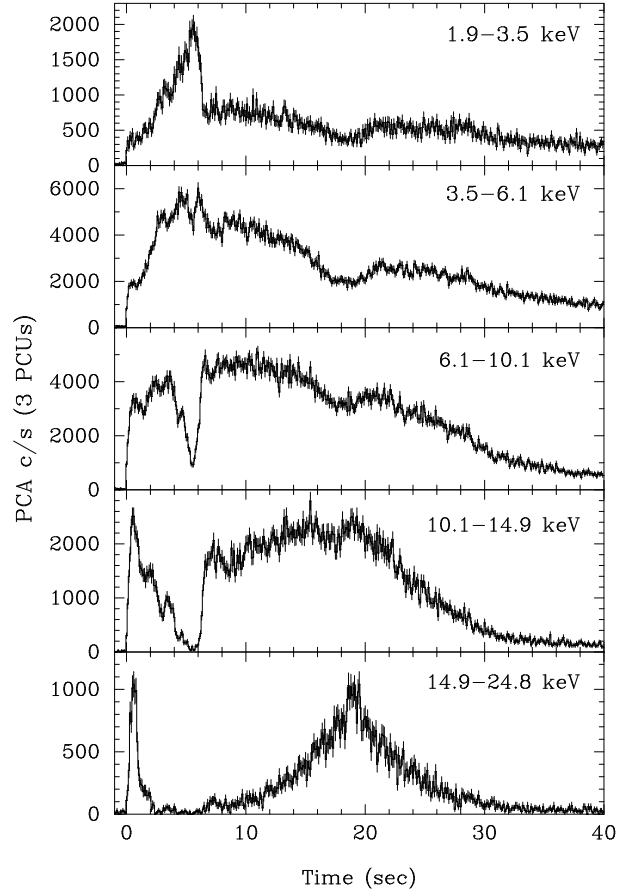


Fig. 2.— The burst light curve, broken down into several bands to show the energy dependence of the profile.

hydrogen column density was poorly constrained by the data, leading us to fix it at a nominal value of $N_H = 7 \times 10^{21} \text{ cm}^{-2}$, consistent with previous observations (e.g. Sidoli et al. 2000). These fits produced acceptable values of χ^2 throughout the burst. No improvements were gained using more sophisticated fitting models that include Comptonization of the blackbody component or modification of the blackbody by electron scattering (Nishimura, Mitsuda, & Itoh 1986; Nakamura et al. 1989), or a contribution from disk reflection of the burst emission (Day & Done 1991). We saw no indications of transient narrow absorption or emission features in the spectra.

In Figure 3, we plot the variation of the bolometric luminosity, the blackbody temperature kT_{bb} , and

the derived apparent blackbody radius R_{bb} through the burst as a function of time. (At the temperatures and densities found on accreting neutron stars, the Compton scattering opacity dominates over the absorption opacity, reducing the emissivity below that expected for a true blackbody. Thus, this method measures the color temperature rather than the effective temperature kT_{eff} . We will return to this point in the Discussion section.) In the lowest panel we see clear evidence for photospheric radius expansion; the apparent radius increases in 5.6s to a maximum envelope radius of $R_{bb}=118\pm 5$ km, followed by an even more rapid collapse to $R_{bb}=29.0\pm 1.5$ km over the next 1.0s. After this point the apparent radius contracts at a more steady rate to a minimum value of 8.6 ± 1.0 km, 20s after the initial burst rise. As is common in radius expansion bursts, the measured blackbody temperature mirrors the behavior of the derived radius. After an initial temperature peak during the first 1.0s of the burst, the temperature drops sharply during the photospheric expansion phase. During the subsequent contraction, the temperature climbs back to its peak value of $kT_{bb}=2.70\pm 0.13$ keV, and then cools exponentially as the blackbody radius stabilizes. In calculating the luminosity we assume that the radiation is isotropic and that the source is located at a distance of $d=10.4$ kpc (Durrel & Harris 1993; Harris 1996). The luminosity peaks at a value of 6.5×10^{38} erg s $^{-1}$, and over the whole 300s interval where the effects of the burst are detectable, the total integrated burst energy is 1.85×10^{40} ergs.

While it is common practice in burst spectral studies to subtract off the continuum emission prior to fitting, it is well-known that this is a source of potential error (e.g. Lewin et al. 1993). If there are two components to the persistent emission, and one component originates on the neutron star or in the boundary layer around it, this component of the emission may either increase or disappear during the burst itself, meaning that the “continuum background” is either underestimated or overestimated. This can lead to an erroneous decrease in the apparent blackbody radius particularly towards the end of the burst, where the flux level is low. In addition, for bursts that approach or exceed the Eddington limit, the possibility exists that the global accretion onto the neutron star itself may be suppressed, leaving the burst itself as the *only* source of X-ray emission for the brief duration of the burst.

We investigated both of these possibilities to deter-

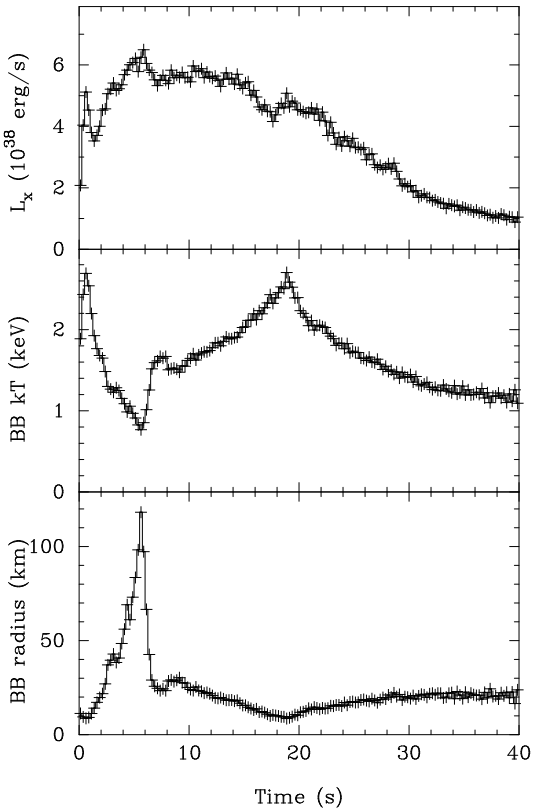


Fig. 3.— The variation of the bolometric luminosity (for a distance of 10.4 kpc), blackbody color temperature kT_{bb} , and apparent blackbody radius R , derived from fits to spectra accumulated through the burst with 0.25s resolution.

mine whether they affect our results. The persistent continuum emission prior to the burst (and, in fact, through the whole RXTE observation) can be well fit using either a straightforward cut-off power law with index $\Gamma=1.63\pm 0.16$, $E_{cut}=8.2\pm 1.8$ keV, $\chi^2=26/36$, or with a combination of a powerlaw plus blackbody, with $\Gamma=2.42\pm 0.11$, $kT_{bb}=1.43\pm 0.16$ keV, $\chi^2=20/35$, with the blackbody providing $\sim 20\%$ of the total flux. In the first formulation, there is no contribution from the region on or around the neutron star; adopting the second, we repeated our series of fits through the burst, holding the powerlaw component constant and allowing the continuum+burst blackbody component to vary. We found that the continuum blackbody contribution was a sufficiently small addition that it had a negligible effect on Figure 3 and on the physi-

cal numbers quoted below. (The broadband 0.1–100 keV spectrum of X2127+119 was found to be well-described by a partially-covered powerlaw plus a disk blackbody (Sidoli et al. 2000); our spectroscopy results are consistent with this model, though the PCA lacks the sensitivity to the lowest energies provided by the SAX LECS instrument that would enable us to perform a detailed study of partial covering over the limited intensity variations found in these data.)

We next repeated our series of burst fits assuming a cessation of persistent emission during the burst, and fitting a blackbody to the overall emission with only the relevant instrumental PCA background subtracted. This produced poor fits to the individual spectra, with large systematic errors in the residuals, indicating that the assumption was invalid and that persistent emission does indeed continue unabated during the burst.

3. Discussion

A comparison of the 1988 and 2000 bursts from X2127+119 shows that there are strong similarities between the two events. Both show multiple peaks in their X-ray light curves in count- and flux- space, and both show indisputable evidence for radius expansion and a qualitatively similar evolution of flux and blackbody temperature and radius. The bursts have peak luminosities of $L_{max}=5.3\times10^{38}$ erg s $^{-1}$ and 6.5×10^{38} erg s $^{-1}$ respectively; peak blackbody temperatures of $kT_{bb}=2.87\pm0.03$ keV and $kT_{bb}=2.70\pm0.13$ keV; and developed from comparable levels of continuum emission ($F_{pers}=5.0\times10^{-10}$ erg cm $^{-2}$ s $^{-1}$ and $F_{pers}=4.2\times10^{-10}$ erg cm $^{-2}$ s $^{-1}$ over the 1–28 keV range) (Dotani et al. 1990, van Paradijs et al. 1990, and above, assuming $d=10.4$ kpc).

The bursts differ in the maximum extent of their photospheric expansion – $R_{bb}\sim1000$ km and $R_{bb}\sim120$ km respectively – and in their timescales. The 1988 burst reached its maximum radius expansion after ~6 s, the end of its sharp radius contraction after ~18 s, and final photospheric touchdown (as defined by the simultaneous peak in kT_{bb} and trough in R_{bb}) after ~90 s. For the 2000 burst these times are respectively 5.6s, 6.6s, and ~19 s. The e-folding time for the decay of the 1988 burst is hard to determine from van Paradijs et al. (1990), but they note that the burst intensity had decreased to 20% by 160s after burst onset. For the 2000 burst, the 20% mark is reached after 38s. Largely due to this difference

in timescales, the total bolometric energy released by the bursts differs by a factor of 4: 6.3×10^{40} ergs for the 1988 event, as compared to 1.85×10^{40} ergs for the 2000 event. Although a little weaker than the first burst, the burst described here still ranks as an unusually energetic event.

From the fluxes derived earlier we calculate the burst characteristics γ ($=F_{pers}/F_{max}$) and τ ($=E_b/F_{max}$, where E_b is the total burst fluence or integrated net flux across the burst) to be 0.0125 and 125s respectively for the 1988 burst, and 0.0084 and 28.5s for the burst presented above. In their summary of the properties of Eddington-limited bursts from a large number of sources, van Paradijs, Penninx & Lewin (1988) find a strong anti-correlation between $\log \tau$ and $\log \gamma$ for Type I bursts showing photospheric radius expansion. The X2127+119 bursts lie on the line of this anti-correlation, but at the extreme end of the (γ, τ) distribution, indicating the intensity and long duration of the bursts from X2127+119 relative to those from other sources.

In Figure 4a we present the luminosity-temperature ($L_{bol}-kT_c$) diagram for the 2000 burst, constructed using the parameters derived from the fits to the spectra out to 100s after the burst rise. The radius expansion and contraction phases are almost horizontal at a luminosity corresponding to the Eddington limit, with a slope introduced by general relativistic effects. Figure 4a can be directly compared to the equivalent diagram for the 1988 burst (van Paradijs et al. 1990, Figure 9); in removing the time domain, this representation emphasises the similarity between the two bursts. Figure 4b shows the strong inverse correlation between the apparent blackbody radius and temperature; the track defined by the envelope contraction lies almost on top of the expansion track, indicating the reversibility of the thermodynamic processes involved. From first principles the luminosity, radius, and temperature of the photosphere should be related by the expression $L = 4\pi\sigma R^2 T^4$. In this case the luminosity is not quite constant, and the radius and temperature obey the relation $R \propto T^{-\alpha}$, with $\alpha=2.06\pm0.04$ (90% confidence). Both diagrams show the radiative cooling curve of the neutron star surface after the touchdown of the photosphere.

While a simple blackbody often provides reasonable fits to burst spectra from neutron stars, the energy distribution of the 'true' emission is likely to be more complex. A systematic difference is expected between the blackbody color temperature kT_c ($=kT_{bb}$)

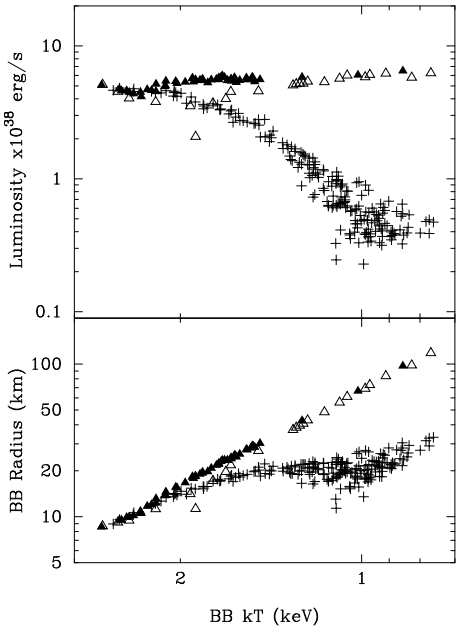


Fig. 4.— The data from Figure 3, extended out to 100s after the burst rise, and replotted to show the (a) luminosity-temperature diagram, (b) radius-temperature diagram. Data from the radius expansion (0s–6s), envelope contraction (6s–19s) and black-body cooling curve (19s–100s) are plotted with open triangles, filled triangles, and crosses respectively. Note the almost-horizontal track in the upper diagram corresponding to the probable Eddington luminosity of the source, and the close correspondence between the expansion and contraction profiles in each diagram.

obtained from spectral fitting and the effective temperature kT_{eff} , due to the dominant contribution of electron scattering in the hot neutron star atmosphere, and the resulting suppression of emissivity (van Paradijs 1982). Model atmosphere calculations show that the spectral hardening ratio $t=T_c/T_{eff}$ is greater than 1, and increases as a function of T_{eff} and of $l=L_x/L_{Edd}$ (London et al. 1984, 1986; Ebisuzaki & Nomoto 1986, 1988; Titarchuk 1994; Madej, 1997). The neutron star radius observed by a distant observer, R_∞ , is related to R_{bb} by $R_\infty=R_{bb}t^2$. Accurate knowledge of the behavior of t would place direct constraints on the mass-radius relationship for neutron stars. However, there is as yet no convincing agreement between the various existing theoretical models,

and in addition the model atmosphere calculations do not match the observed variations with luminosity in several sources, including X1608–522 (Penninx et al. 1989) and X2127+119 itself (see below, and Figure 5). If we adopt a representative spectral hardening factor of $t=1.5\pm0.1$ (e.g. London et al. 1984, 1986; Madej 1997) for illustrative purposes, our measured photospheric touchdown radius of $R_{bb}=8.6\pm1.0$ km would imply $R_\infty=19.3\pm3.4$ km.

The value of the Eddington luminosity measured by a distant observer depends upon the mass and radius of the emitting object. In the limiting case, the Eddington luminosity measured at very large photospheric radii, $L_{Edd,\infty}(R \gg R_*)$, will be greater than the value measured at the point of photospheric touchdown, $L_{Edd,\infty}(R = R_*)$, by a factor equivalent to the gravitational redshift at the neutron star surface, $1 + z_*$ (Paczynski & Anderson 1986; Damen et al. 1990). At intermediate radii, the ratio of the Eddington luminosities observed ($L_{Edd,\infty}(R > R_*)/L_{Edd,\infty}(R = R_*)$) is a function of both the redshift and photospheric radius, as modified by the (possibly varying) spectral hardening (Damen et al. 1990). Therefore, the photospheric expansion track allows us to directly estimate the gravitational redshift factor at the surface of the neutron star, if we account correctly for the finite size of the photosphere and for the temperature dependence of the scattering opacity mentioned above.

For each data point in the photospheric expansion track (Figure 4a), we applied Eqns. 7–9 of Damen et al. (1990) to obtain an instantaneous estimate of $(1 + z_*)$, and then took the mean of these derived values. For this calculation we adopted an Eddington luminosity at touchdown of $L_{Edd,\infty}(R = R_*)=(5.08\pm0.31)\times10^{38}$ erg s^{−1} and a temperature at touchdown of 2.70 ± 0.13 keV.

Model atmosphere calculations during the expansion phase of a burst have not yet been performed, so we calculated the redshift for two differing assumptions. First, we assumed that the spectral hardening ratio was constant during the expansion, and thus that no correction was required for non-Planckian shape of the burst spectra. For this case, we obtained a value of $1 + z_* = 1.17\pm0.05$ (s.d.). In the second derivation we assumed (again following Damen et al. 1990) that the dependence of t on the observed color temperature $T_{c,\infty}$ is the same during radius expansion and contraction as it is during the neutron star cooling. We cannot derive absolute values for t

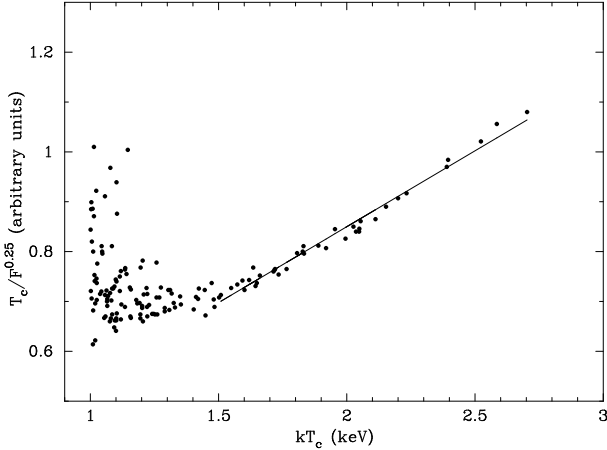


Fig. 5.— The variation of the spectral hardening factor $t=T_c/T_{eff} \propto T_c/F_0^{0.25}$, as a function of the color temperature T_c derived from spectral fits. The best-fitting straight line for the higher-temperature data points is overlayed.

from observational data alone; we can, however, determine *relative* values, and this is all the method requires. During cooling, the effective temperature $T_{eff,\infty}$ is proportional to $F_\infty^{0.25}$, and thus the hardening factor t is proportional to $T_{c,\infty}/F_\infty^{0.25}$ (Penninx et al. 1989; Damen et al. 1990). In Figure 5 we show $T_{c,\infty}/F_\infty^{0.25}$ plotted against $T_{c,\infty}$ for the cooling track of our X2127+119 burst, following photospheric touchdown. For temperatures $kT_c > 1.5$ keV, the relationship can be approximated with a straight-line fit. Using this fit to scale the radius estimates that enter the redshift calculation (Damen et al. 1990, Eqn. 9), our derived gravitational redshift factor becomes $1+z_* = 1.28 \pm 0.06$ (s.d.).

Applying the relativistic correction and solving for L_{Edd} and mass (e.g. Lewin et al. 1983, van Paradijs et al. 1990), we then obtain, for the constant- t case, a corrected Eddington luminosity of $L_{Edd,\infty}(R \gg R_*) = (5.94 \pm 0.45) \times 10^{38}$ erg s $^{-1}$ and a neutron star mass of $M = 2.38 \pm 0.18(1+X)M_\odot$, where X is the hydrogen content by mass; $X=0$ for hydrogen-poor material and $X=0.73$ for cosmic composition). For the variable- t instance, these values are $L_{Edd,\infty}(R \gg R_*) = (6.50 \pm 0.50) \times 10^{38}$ erg s $^{-1}$ and $M = 2.60 \pm 0.22(1+X)M_\odot$.

We emphasise that although only statistical errors are quoted here, all current derivations of basic neu-

tron star parameters from burst spectroscopy are affected by the systematic uncertainties in the interpretation of the spectral fit temperatures (van Paradijs et al. 1990, Lewin et al. 1993). Our own data (Figure 5) imply a possible variation in t of $\sim 50\%$ over the temperature range $1.5 > kT_c > 2.7$ keV which is not well reproduced in the model atmosphere calculations. The composition of the accreted matter, and degree of anisotropy in the burst radiation, are additional key unknowns limiting our ability to obtain the mass-radius relationship of the neutron star using these methods.

Nonetheless, while higher than canonical, the values of L_{Edd} and M derived here are consistent with those obtained by van Paradijs et al. (1990) for the 1988 burst. It therefore seems likely that the only significant difference between the two bursts is in the overall timescale of the burst, and thus the total amount of matter ignited in the thermonuclear flash. The quantity of energy liberated in the combustion of hydrogen and helium into iron-peak elements depends on the ratio of the original mix. Following Lewin et al. (1993) and adopting a conversion fraction of 6×10^{18} erg g $^{-1} = 0.007c^2$, we calculate that the two events respectively consumed 1.1×10^{22} g and 2.8×10^{21} g of accumulated material, each equivalent to many days of accretion from the secondary.

We thank Cynthia Hess, Erik Kuulkers, and Tod Strohmayer for useful comments and discussions.

REFERENCES

- Aurière, M., Le Fèvre, O., & Terzan, A., 1984, A&A, 138, 415
- Bradt, H.V., Rothschild, R.E., & Swank, J.H., 1993, A&AS, 97, 355
- Damen, E., Magnier, E., Lewin, W.H.G., Tan, J., Penninx, W., & van Paradijs, J., 1990, A&A, 237, 103
- Day, C.S.R., & Done, C., 1991, MNRAS, 253, 35P
- Durrel, P.R., & Harris, W.E., 1993, AJ, 105, 1420
- Dotani, T., Inoue, H., Murakami, T., Nagase, F., Tanaka, Y., Tsuru, T., Makishima, K., Ohashi, T., & Corbet, R.H.D., 1990, Nature, 347, 534
- Ebisuzaki, T. & Nomoto, N., 1986, ApJ, 305, L67
- Ebisuzaki, T. & Nomoto, N., 1988, ApJ, 328, 251

Fabian, A.C., Pringle, J.E., & Rees, M., 1975, MNRAS, 172, 15P

Geisler, D., Minniti, D., Claria, J.J., 1992, AJ, 104, 627

Harris, W.E., 1996, AJ, 112, 1487

Hoffman, J.A., Cominsky, L., & Lewin, W.H.G., 1980, ApJ, 240, L27

Homer, L., & Charles, P.A., 1998, New Astron. 3/7, 435

Hut, P., McMillan, S., Goodman, J., Mateo, M., Phinney, E.S., Pryor, C., Richer, Harvey B., Verbrunt, F., & Weinberg, M., 1992, PASP, 104, 981

Ilovaisky, S.A., Aurière, M., Koch-Miramond, L., Chevalier, C., Cordoni, J.-P., & Crowe, R.A., 1993, A&A, 270, 139

Jahoda, K., Swank, J. H., Giles, A. B., Stark, M. J., Strohmayer, T., Zhang, W., & Morgan, E. H., 1996, in EUV, X-ray and Gamma-Ray Instrumentation for Astronomy VII, ed O. H. Siegmund (Bellingham, WA: SPIE), 59

Lewin, W.H.G., van Paradijs, J., & Taam, R.E., 1993, SSR, 62, 223

London, R.A., Taam, R.E., & Howard, W.M., 1984, ApJ, 287, L27

London, R.A., Taam, R.E., & Howard, W.M., 1986, ApJ, 306, 170

Madej, J., 1997, A&A, 320, 177

Nakamura, N., Dotani, T., Inoue, H., Mitsuda, K., Tanaka, Y., & Matsuoka, M., 1989, PASJ, 41, 617

Nishimura, J., Mitsuda, K., & Itoh, M. 1986, PASJ, 38, 819

Paczyński, B., & Anderson, N., 1986, ApJ, 302, 1

Penninx, W., Damen, E., Tan, J., Lewin, W.H.G., & van Paradijs, J., 1989, A&A, 208, 146

Sidoli, L., Parmar, A.N., & Oosterbroek, T., 2000, A&A, 360, 520

Sneden, C., Kraft, R.P., Prosser, C.F., & Langer, G.E., 1991, AJ, 102, 2001

Titarchuk, L., 1994, ApJ, 429, 340

van Paradijs, J., 1982, A&A, 107, 51

van Paradijs, J., Dotani, T., Tanaka, Y., & Tsuru, T., 1990, PASJ, 42, 633

van Paradijs, J., Penninx, W., & Lewin, W. H. G. 1988, MNRAS, 233, 437